fire

MDPI

Article

Smoke Blocking by Water Mist Curtains in Tunnel Fires: A Parametric Study and Momentum-Ratio Criterion

Jiayun Sun [1,2], Zhenyu Guo [1] and Junheng Wang [1,2,*]

[1] School of Chemistry and Environmental Engineering, Wuhan Textile University, Wuhan 430200, China
[2] Hubei Key Laboratory for Clean Recycling and Resource Utilization of Waste Fibers, Wuhan Textile University, Wuhan 430200, China
* Correspondence: wangjunheng@whu.edu.cn

Abstract

Controlling fire-induced smoke in tunnels remains a critical issue in tunnel fire safety. This study investigates the use of a water mist curtain to contain fire-induced heat and smoke through small-scale experiments and Fire Dynamics Simulator (FDS) modeling. Reduced-scale tunnel tests first show that a properly arranged water mist curtain can limit the downstream spread of hot smoke under natural ventilation. Full-scale simulations are then used to examine the effects of the number of nozzles per row, row spacing, and total water flow rate for heat release rates (HRRs) from 1000 to 5000 kW. The results indicate that, when the total water flow rate is low, i.e., the water mist curtain is insufficient to block smoke, changing the nozzle arrangement has only a limited effect on downstream temperature, although the upward flow becomes stronger with more nozzles per row. Increasing the total water flow rate enhances the cooling effect and induces a reverse-flow region near the water mist curtain, making it more difficult for fire-induced smoke to pass through the water mist zone. Based on the theoretical analysis and simulation results, a dimensionless momentum ratio (the water-mist momentum to the smoke momentum), $R = \frac{M_w}{M_s}$, is proposed to evaluate the smoke blocking effect of water mist curtains. A critical value of $R = 24$ is identified for the tested HRR, water mist curtain and tunnel geometry.

Keywords: tunnel fire; water mist curtain; smoke blocking effect; dimensionless momentum ratio; FDS

1. Introduction

In recent years, tunnel fire safety has received increasing attention because of the rapid growth of tunnel construction worldwide and several catastrophic tunnel fire incidents [1]. Owing to the limited cross-sectional area of tunnels, hot fire-induced smoke can spread rapidly along the ceiling, either downstream with traffic or under the action of longitudinal ventilation [2–4]. This creates a severe threat to occupants downstream of the fire, who may be exposed to high temperatures [5,6] and toxic gases, particularly in urban tunnels where congestion is common during peak hours. Inspired by the concept of fire compartmentation in buildings [7], a water mist curtain consisting of an array of nozzles was proposed in our previous work [8] as a barrier to limit the spread of fire-induced heat and smoke. Small-scale tunnel fire tests were carried out to evaluate the effectiveness of the water mist curtain under natural ventilation.

Sun et al. conducted a comprehensive investigation of the use of a water mist curtain to prevent the horizontal spread of fire-induced smoke in tunnels [8–10]. Liang et al. [11] demonstrated that water mist screens can enhance smoke extraction efficiency in transversely

Check for updates

Academic Editors: Yuxuan Yang and Zihe Gao

Received: 17 October 2026
Revised: 4 November 2026
Accepted: 10 November 2026
Published: 13 November 2026

Copyright: © 2026 by the authors. Licensee MDPI, Basel, Switzerland. This article is an open access article distributed under the terms and conditions of the Creative Commons Attribution (CC BY) license.

ventilated tunnels, offering a viable alternative to auxiliary air supply. Liu et al. [12] investigated the impacts of the water mist system on heat release rate, smoke temperature, smoke blocking performance and critical velocity, with variables including nozzle position, nozzle row number and nozzle pressure, in a longitudinally ventilated tunnel. The impact of the water mist system on the smoke back-layering length is studied by Gao et al. [13]. They reported that multi-row configurations enlarge the effective mist coverage over the smoke layer and enhance cooling, thereby further suppressing smoke back-layering. Kan et al. [14] carried out full-scale experiments and verified that installed water mist systems can achieve both heat reduction and smoke blocking. Their further research demonstrated that the combined operation of longitudinal ventilation and dual water mist curtains can strengthen smoke confinement and reduce the ventilation rate required for smoke control. Chen et al. [15] numerically demonstrated the barrier performance of mist curtain systems in road tunnel fires. Li et al. [16] tested water mist curtains in a 1:3 scale tunnel model and verified their effectiveness under both natural and longitudinal ventilation, particularly for smaller fires. Wang et al. [17] investigated smoke back-layering under the coupled effects of longitudinal ventilation, tunnel slope, and water spray, establishing a dimensionless correlation incorporating ventilation velocity, heat release rate, spray flow rate, and tunnel slope; their results showed that increasing the spray flow rate progressively reduces the smoke back-layering length under longitudinal ventilation.

As water mist(spray) systems have been widely adopted in tunnels, their performance in fire extinguishment [14,18–22] and influence on smoke flow characteristics inside tunnels [15,23–26] have been investigated. However, it can be seen from the above literature review that investigations into using water mist or sprays to suppress smoke spread remain scarce. In particular, given that the configurations of water mist(spray) systems and their characteristic parameters vary from one study to another, the applicability of relevant research findings is limited.

In our previous studies [8–10], the effectiveness of using a water mist curtain to block the fire-induced smoke in tunnels was preliminarily verified by small-scale experiments, and the induced flow fields were interpreted by means of CFD simulations. However, the performance of the water mist curtain in full-scale tunnel models has not been investigated. In order to address this gap, a series of full-scale simulations is carried out in the present study, along with a systematic parametric investigation of the fire characteristic parameter (HRR), nozzle arrangement, row spacing, and total water flow rate. Moreover, the critical conditions under which a water mist curtain can suppress the horizontal spread of smoke are explored, based on theoretical analysis and experimental and numerical results.

2. Theoretical Analysis

When a fire occurs in a tunnel, buoyant smoke rises and impinges on the tunnel ceiling. After impingement, the smoke spreads horizontally along the ceiling as a ceiling jet until it reaches the water mist curtain. The water mist curtain is formed by multiple high-pressure nozzles arranged across the tunnel section. As water droplets discharge downward from the nozzles, they entrain the surrounding air and fire-induced smoke into the spray region, thereby limiting further smoke propagation, as shown in Figure 1.

The smoke-blocking performance of the water mist curtain is governed by the interaction between the downward droplet momentum and the horizontal momentum of the ceiling jet. Since it is difficult to experimentally resolve the velocity and mass of individual droplets, the droplet momentum of the water mist curtain is estimated from the nozzle flow rate and the mean jet velocity. For N identical nozzles, the downward momentum flux of the water mist curtain can be written as

$$M_w = N\rho_w \frac{Q_n^{\,2}}{A_n} = N\rho_w Q_n v_j \tag{1}$$

where Q_n is the volume flow rate per nozzle, $An = \pi d_n^2/4$ is the nozzle orifice area, d_n is the nozzle orifice diameter, $v_j = Q_n/A_n$ is the mean jet velocity at the nozzle exit, and ρ_w is the water density.

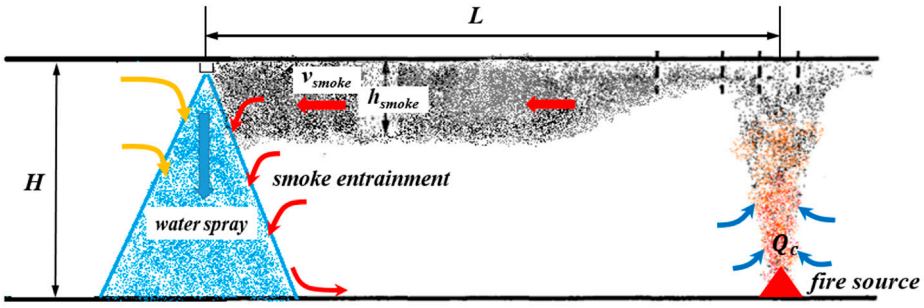

Figure 1. Sketch of the interaction between the smoke layer and water mist curtain in a tunnel configuration.

The horizontal momentum flux of the ceiling jet can be expressed as

$$M_s = \rho_s W h_s v_s^2 \tag{2}$$

where W is the tunnel width, h_s is the smoke-layer thickness, ρ_s is the smoke density, and v_s is the representative horizontal velocity of the smoke layer. For a fixed water mist curtain, the downward water-mist momentum is approximately constant; therefore, a larger smoke mass flow rate or a higher ceiling-jet velocity reduces the relative effectiveness of the curtain. A higher smoke propagation velocity also shortens the contact time between smoke and droplets, weakening droplet entrainment and cooling.

For the steady ceiling-jet region (L/H > 1.523), the maximum ceiling-jet velocity may be estimated using a correlation of the following form [2]:

$$v_s = 0.5812 Q_c^{*1/3} \cdot \sqrt{gH} \cdot \left(\frac{l_b}{H}\right)^{-\frac{1}{3}} exp\left(-0.0237 \cdot \frac{L}{H} \cdot \left(\frac{l_b}{H}\right)^{\frac{1}{3}}\right), \tag{3}$$

where

$$Q_c^* = Q_c/(\rho_\infty C_p T_\infty g^{\frac{1}{2}} H^{\frac{5}{2}}),$$

Q_c is the convective heat release rate, l_b is half of the tunnel width, H is the tunnel height, and L is the horizontal distance from the center of the fire source to the water mist curtain.

We propose a new dimensionless momentum ratio, R, defined as the ratio of the momentum of the water mist curtain to that of the fire-induced ceiling jet, to evaluate the relative ability of the water mist curtain to restrain the horizontal ceiling jet:

$$\mathrm{R} = \frac{M_w}{M_s}. \tag{4}$$

A larger R indicates a stronger water mist curtain relative to the approaching smoke momentum and therefore a higher potential for smoke blocking.

3. Experimental and Numerical Models

3.1. Experimental Setup

Since this paper mainly focuses on the smoke blocking effect of the water mist curtain without longitudinal ventilation, only the experimental configuration and results obtained under natural ventilation are summarized here.

The small-scale tunnel was 18 m long, 1.1 m wide, and 0.4 m high. The tunnel boundaries were constructed from 8 mm thick non-combustible fire-rated glass. The water mist curtain was installed across the tunnel section. Several nozzle rows were arranged from upstream to downstream, with row spacings of 0.3 m and 0.6 m. The maximum water flow rate was 1.94 L/min and the maximum operating pressure was 0.65 MPa. Thermocouples were installed along the tunnel at intervals of 1.5 m and at heights of 0.04, 0.20, and 0.36 m. The detailed tunnel and nozzle arrangements are shown in Figure 2.

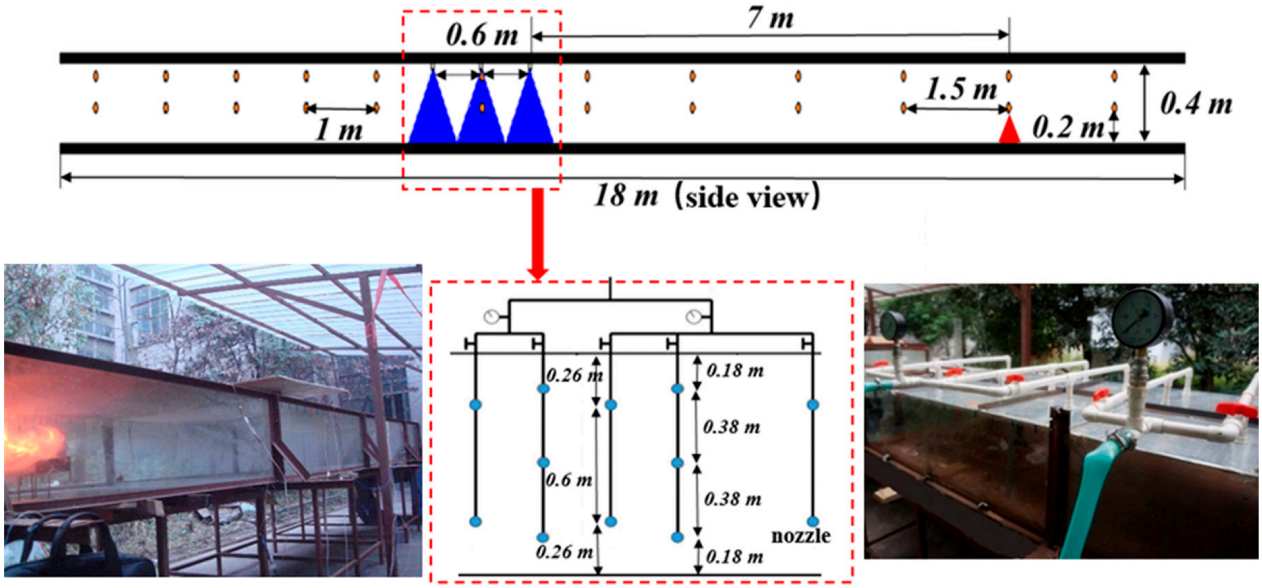

Figure 2. Side view and bird's-eye view of the sketch of the tunnel and the nozzle system layout.

3.2. Scaling Methodology

A suitable scaling method is required to transfer small-scale results to full-scale conditions. Several scaling techniques are available, but Froude scaling is the most commonly used for fire-induced flows. In the present study, the geometric scale ratio was set to 1:10. Accordingly, the full-scale tunnel dimensions were 180 m × 11 m × 4 m. The solid tunnel surfaces were represented using the same thermophysical properties as in the small-scale simulations. The ambient temperature was set to 20 °C. Twenty thermocouples were defined in the mid-vertical plane at x = 5.6 m, distributed every 15 m along the tunnel in a manner consistent with the small-scale configuration. According to Heskestad [20], the droplet momentum should be reproduced across scales for droplet–flow interactions, which yields the water droplet diameter that scales as $L^{1/2}$. Table 1 summarizes the scaling laws and input parameters.

Table 1. Scaling laws and input parameters [20,27].

Parameters and Units	Scaling Laws	Small-Scale	Full-Scale
HRR (kW)	$L^{5/2}$	15.6	5000
Time (s)	$L^{1/2}$	1	3.16
Temperature (°C)	L^{0}	1	1
Water flow rate (L/min)	$L^{5/2}$	1.94	613
Droplet diameter (μm)	$L^{1/2}$	390	1233

The nozzle orifice and spray characteristics were scaled to represent the full-scale water mist curtain. The full-cone spray angle was 74°. A Rosin–Rammler droplet-size distribution was used with the same shape parameter, γ = 3.0. It should be emphasized that Froude

scaling cannot simultaneously preserve all water-mist processes, including droplet breakup, evaporation, radiation, combustion, and turbulence–droplet interactions; therefore, the scaling assumptions are discussed as a limitation of the present study.

3.3. FDS Setup

The FDS 6 solver was used with the default model settings for turbulence, combustion, and radiation. The radiative fraction was set to 0.17 [28]. Figure 3 shows the heat release rate as a function of time in the small-scale and full-scale simulations; the shaded region indicates the steady-state period used for averaging temperatures and flow fields.

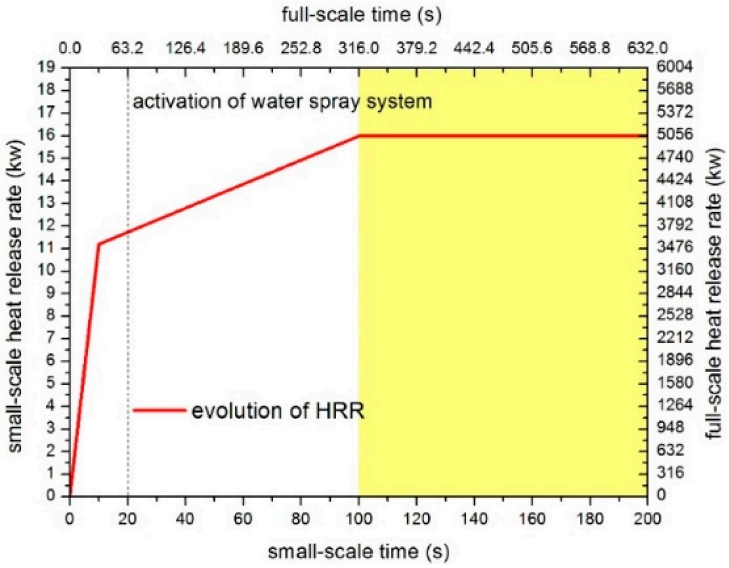

Figure 3. Heat release rate as the function of time in small-scale and full-scale simulations; the yellow area indicates the steady-state period in simulations.

Approximately 50 cases were simulated, including small-scale experiments and full-scale simulations. The HRR ranged from 1000 to 5000 kW. The detailed test settings are listed in Table 2. Cases S-1 to S-3—reduced-scale simulations mirroring the small-scale experiments, used for model validation. Cases F-1 to F-3—full-scale baseline simulations examining the scaling behavior. Cases F-4 to F-45—full-scale parametric simulations varying the nozzle arrangement, row spacing, total water flow rate, and HRR, used for the criterion development.

Table 2. Overview of test settings.

No.	Tunnel Geometry W × H	HRR (kW)	Droplet Diameter (μm)	Flow Rate Per Nozzle (L/min)	Nozzle Combination (Number of Nozzles × Rows)	Row Spacing (m)
S-0	1.1 × 0.4	16.7	/	/	/	/
S-1			390	1.94	2 × 2	0.3
S-2			390	1.94	2 + 3	0.3
S-3			390	1.94	3 × 2	0.3
F-1	11 × 4	5000	1200	613	2 × 2	3
F-2			1200	613	2 + 3	3
F-3			1200	613	3 × 2	3
F4–F45	7 × 4.5	1000, 1500, 2000, 2500, 3000, 5000	160	7.1	6 × 2, 4 × 3, 3 × 4, 2 × 6, 6 × 3, 6 × 4, 6 × 6, 6 × 7, 6 × 8, 6 × 9	3–6

3.4. Mesh Sensitivity

In our previous work [10], an extensive mesh sensitivity study was performed, leading to the conclusion to use a uniform 0.015 m × 0.015 m × 0.015 m mesh for the CFD calculations. This is in line with the well-known D* criterion [29] for fire plumes.

$$D^* = \left(\frac{\dot{Q}}{\rho_\infty T_\infty c_p \sqrt{g}}\right)^{2/5}.$$

A sufficient number of grid cells was also maintained across the tunnel height [30]. The smoke layer was considered adequately resolved by the adopted mesh, and the results were treated as mesh-insensitive for the purposes of the present study. Model validation is presented in Section 4.1, where the differences between simulated and measured temperatures are shown to be acceptable.

4. Results and Discussion

4.1. Model Validation

Figure 4 compares the temperature and flow fields in the vertical plane and Figure 5 compares the temperature and flow fields in the horizontal mid-plane for test S-1.

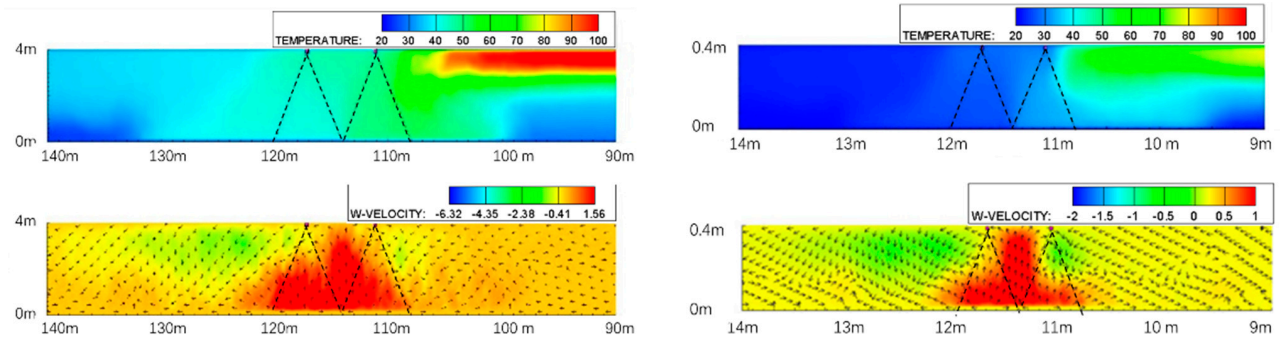

Figure 4. Temperature and flow field in the vertical plane, **left**: x = 5.6 m, **right**: x = 0.56 m, for test S-1. Values have been averaged over the steady-state period.

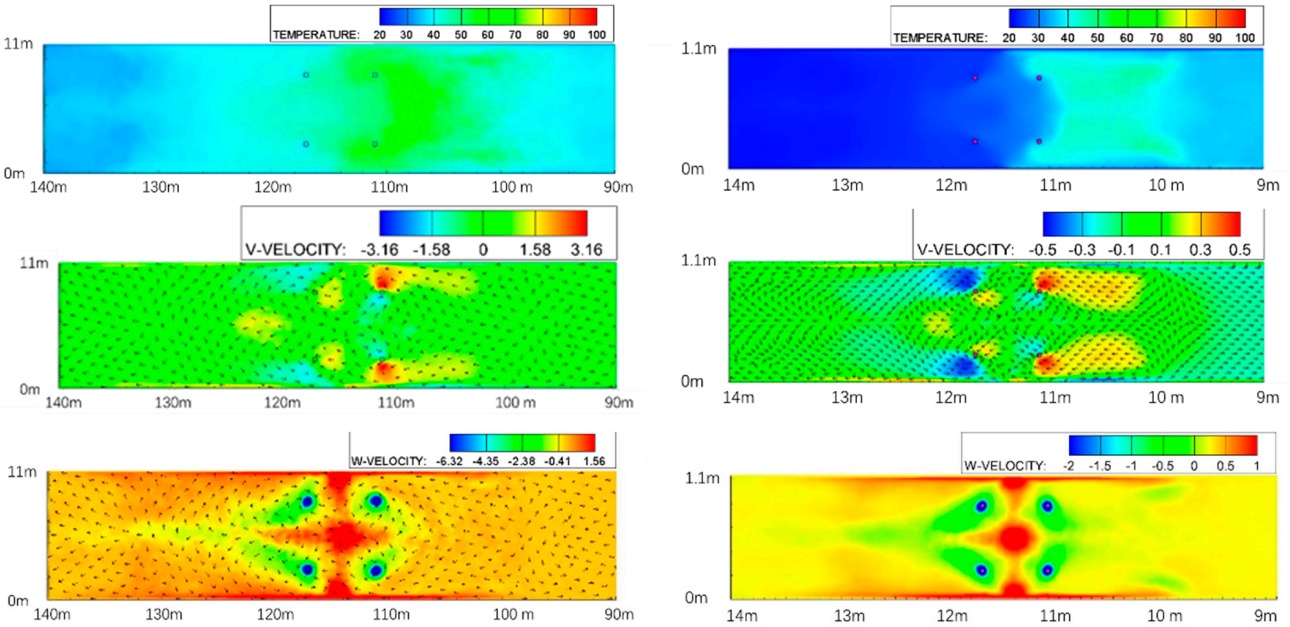

Figure 5. Temperature and flow field in the mid-horizontal planes, **left**: full-scale model, **right**: small-scale model, for test S-1. Values have been averaged over the steady-state period.

The left and right columns correspond to x = 5.6 m in the full-scale model and x = 0.56 m in the small-scale model, respectively. All values were averaged over the steady-state period. Higher temperatures are observed in the full-scale simulations than in the small-scale simulations, both upstream and downstream of the water mist curtain. Nevertheless, the cooling effect of the water mist curtain is also shown in the full-scale simulation results. The flow fields show similar flow patterns: the upward flow occurs in-between the adjacent sprays, while the downward flow occurs beneath the nozzle heads. And the longitudinal velocity component indicates that entrainment near the nozzle heads is slightly stronger in the full-scale results than in the small-scale results.

Figure 6 shows the temperature evolutions for test S-1 in the small-scale and full-scale simulations. The time is scaled according to Froude scaling. Consistent with Figures 4 and 5, higher temperatures are observed in the full-scale simulations. The upward flow in-between adjacent water sprays, which is considered important for the smoke blocking effect, is still captured in the full-scale model. Small temperature deviations are observed near the fire source, and these deviations become larger at position 7, closer to the water mist curtain.

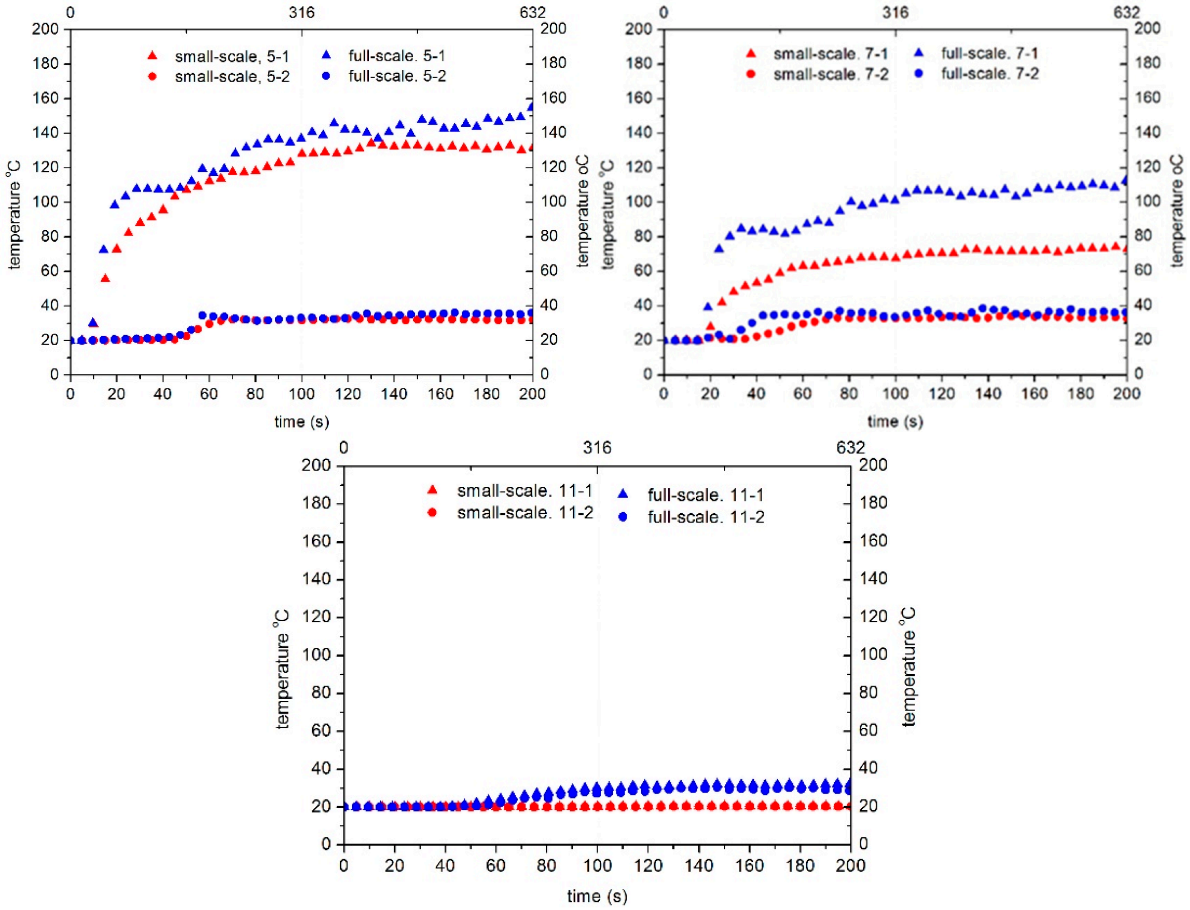

Figure 6. Temperature evolutions of test S-1 in small-scale and full-scale simulations.

As mentioned above, it is not possible to fulfill all scaling laws simultaneously for the interaction between water mist and fire smoke. In the present study we adopted Froude similarity, which implies that the flows are assumed to be Reynolds-number-independent. These simplifications may contribute to deviations in temperature fields. The relative errors observed between the small-scale and full-scale results are less than 8% at the mid-height plane of the tunnel for each measuring point. A higher deviation is observed at Position 7, which is closer to the water mist region and subjected to more complex flow field and heat transfer processes. The maximum relative error is approximately 30% near the tunnel

ceiling. Therefore, for the regions we focus on in this study, which are far from the water mist curtain, the deviations are acceptable.

4.2. Effect of Nozzle Arrangements/Coverage of the Water Mist

In the water mist curtain, the spray generated by each nozzle has a finite conical envelope. Because the spray envelopes do not overlap completely, air gaps exist between adjacent sprays. These uncovered regions may provide pathways for the horizontal propagation of fire-induced smoke. Therefore, this section investigates the effect of spray coverage on the smoke blocking effect.

The total water flow rate was kept constant. Twelve nozzles were considered in four arrangements: 6 nozzles × 2 rows, 4 nozzles × 3 rows, 3 nozzles × 4 rows, and 2 nozzles × 6 rows. The spray region was simplified as a combination of triangular spray envelopes. The nozzle spacing and tunnel dimensions are illustrated in Figure 7. The spray cone angle was 74°.

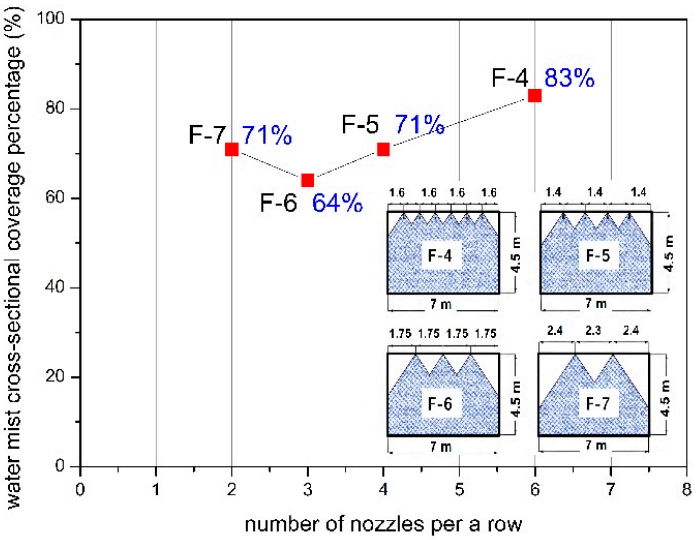

Figure 7. Sketch of the coverage of water mist on tunnel cross-section of tests F-4–7.

The estimated cross-sectional spray coverage is shown in Figure 7. When nozzles are uniformly arranged, increasing the number of nozzles in a single row does not necessarily increase the spray-covered area. As we can see, with an increase in the number of nozzles per row, the spray-covered areas first decrease and then increase, from 71% to 64% and then to 83%.

Figure 8 shows the temperature field in the horizontal plane at z = 4.4 m for tests F-4–F-7. A clear temperature rise downstream of the water mist curtain is observed. Figure 9 presents the temperature evolutions at positions 5 and 6, located upstream of the water mist curtain, and positions 8–10, located downstream. Consistent with Figure 8, the temperature rise behind the water mist curtain is evident. However, the temperature differences among the tested nozzle arrangements do not follow a single monotonic trend. A larger number of nozzles per row does not result in lower downstream temperatures. The maximum temperature for the 6 nozzles × 2 rows arrangement is higher than that for the 4 nozzles × 3 rows arrangement at position 9 (37 °C compared with 30 °C). However, the temperature difference among these tests is limited, with a maximum difference of less than 23%. Nevertheless, a delay in the onset of the downstream temperature rise is observed as the number of nozzle rows increases. This delay is beneficial because it extends the available safe egress time for occupants downstream of the fire.

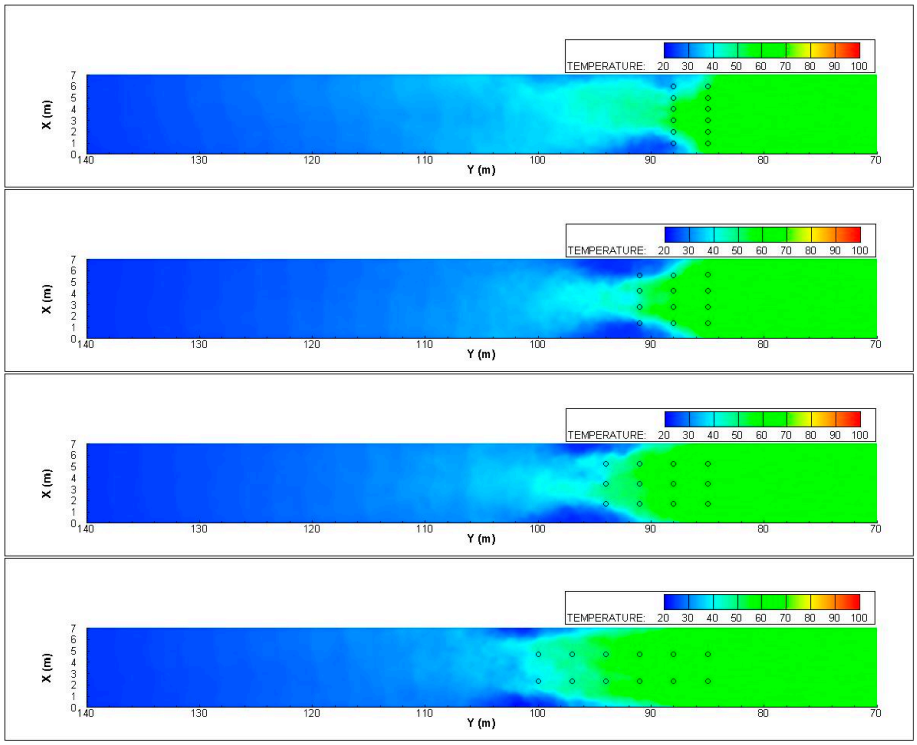

Figure 8. Temperature field in the horizontal plane (z = 4.4 m) for tests F-4–7 (from **top** to **bottom**). Values have been averaged over the steady-state period.

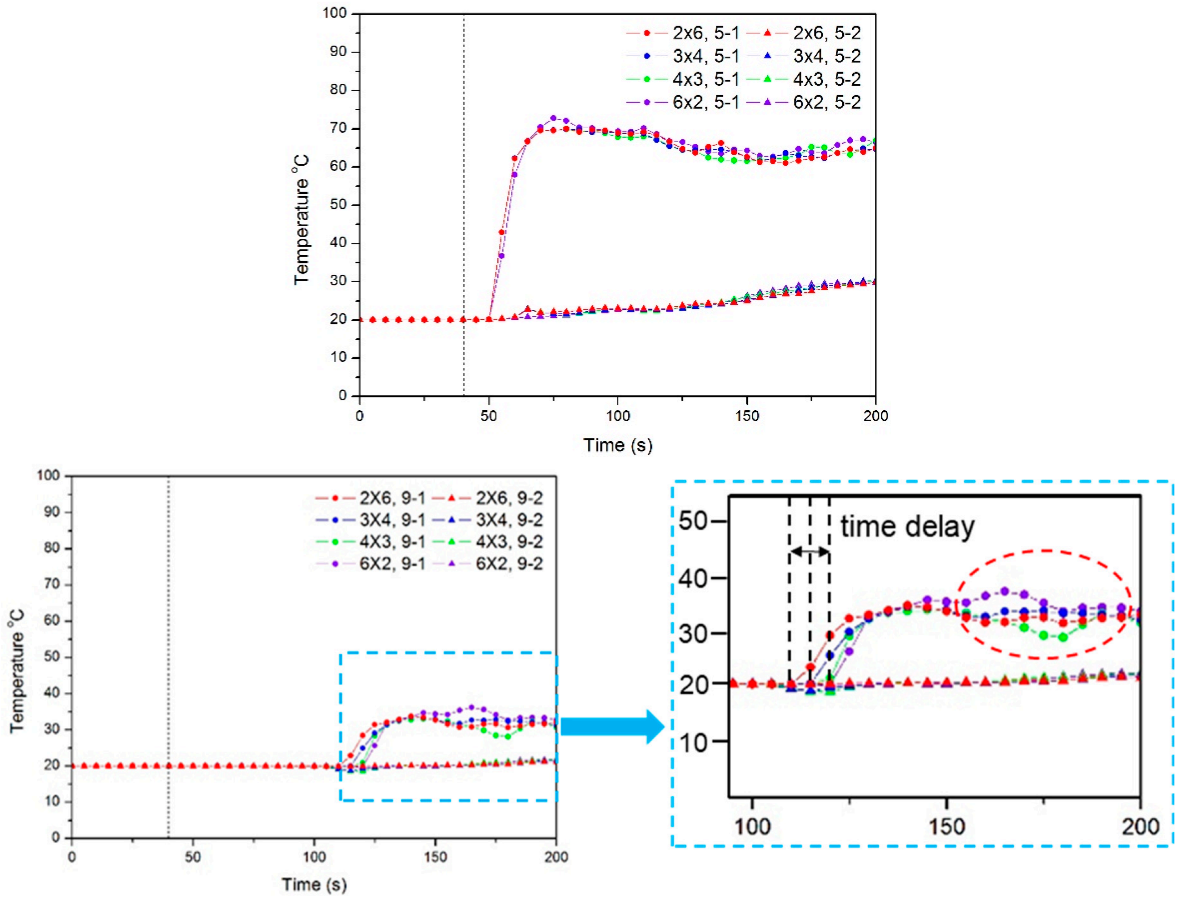

Figure 9. Temperature evolution at positions 5 (close to the fire source), 6 (in between the fire source and the water sprays) and 9 (downstream of the water sprays) for tests F-4–7.

The flow field in the horizontal mid-plane at z = 2.2 m is shown in Figure 10. In contrast to the relatively small temperature differences, stronger upward flow is observed in test F-4, which has more nozzles per row. This suggests that nozzle arrangement affects the local flow structure and entrainment pattern even when its effect on downstream temperature is limited.

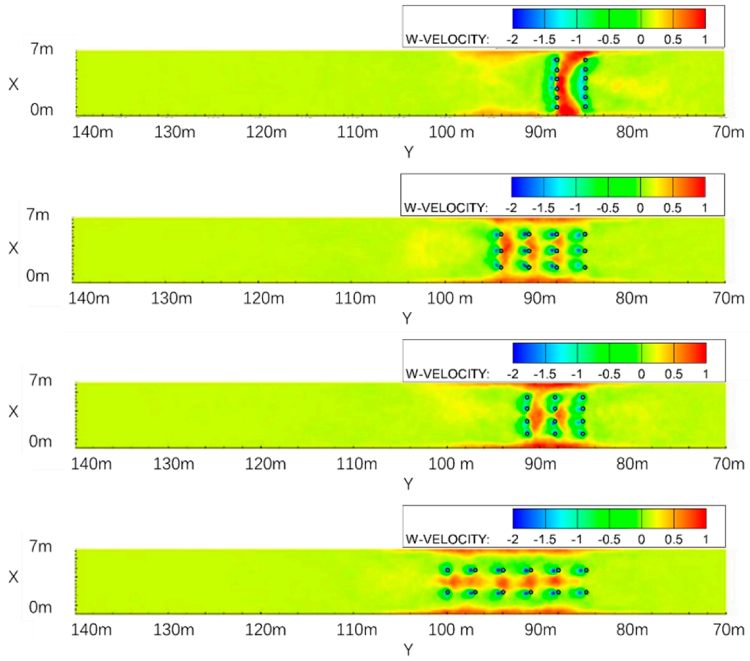

Figure 10. Flow field in horizontal plane (z = 2.2 m) for tests F-4–7 (from **top** to **bottom**). Values have been averaged over the steady-state period.

4.3. Effect of the Row Spacing

Figure 11 shows the temperature fields in the horizontal plane at z = 4.4 m for test F-4 with row spacings of 3 m and 6 m. Figure 12 presents the corresponding temperature and flow fields in the vertical plane at x = 3.5 m.

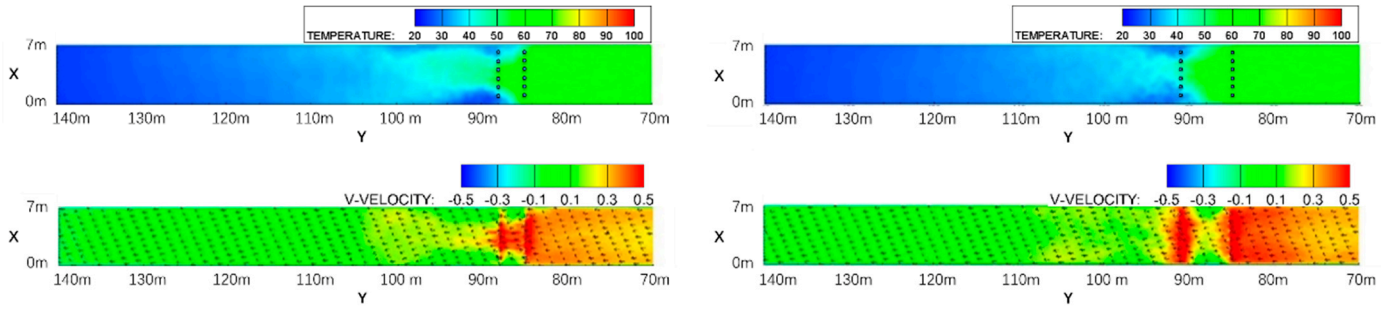

Figure 11. Temperature and flow field in the horizontal plane (z = 4.4 m) for test F-4 (**left**, 3 m; **right**, 6 m). Values have been averaged over the steady-state period.

Note that the protection radius of each nozzle is approximately 3 m. It means partial overlap of adjacent spray zones may occur when the row spacing is 3 m. Higher temperatures are still observed downstream of the water mist curtain, indicating smoke penetration. The longitudinal and vertical velocity components show the effect of row spacing on the flow field. A more pronounced entrainment beneath the nozzles, the downward flow caused by the water mist, and the upward flow between nozzle rows are found for a row spacing of 6 m, because the larger spacing reduces interaction between adjacent sprays.

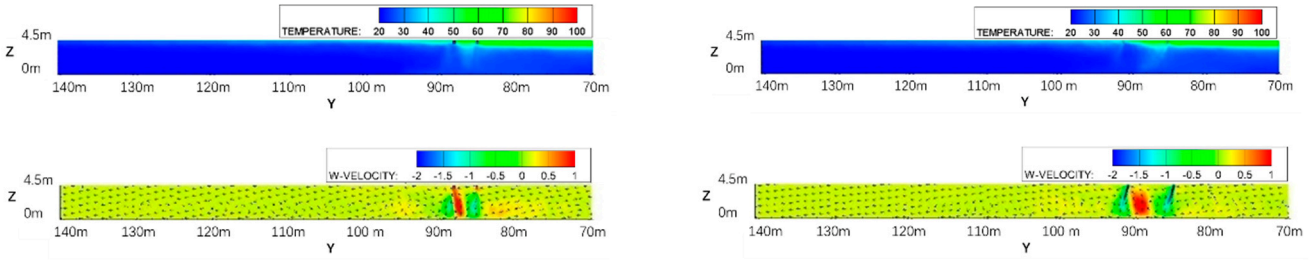

Figure 12. Temperature and flow field in the vertical plane (x = 3.5 m) for test F-4 (**top**, 3 m; **bottom**, 6 m). Values have been averaged over the steady-state period.

Figure 13 shows the temperature evolutions at position 5, upstream of the water mist curtain, and position 8, downstream of the water mist curtain. The temperature difference between the two row spacings is small, although slightly lower temperatures are observed for the 6 m spacing. From this perspective, the strength of the upward flow has only a limited effect on the overall tunnel temperature. The small temperature difference may arise from differences in the relative positions of the measuring points or from differences in the contact time between smoke and water droplets.

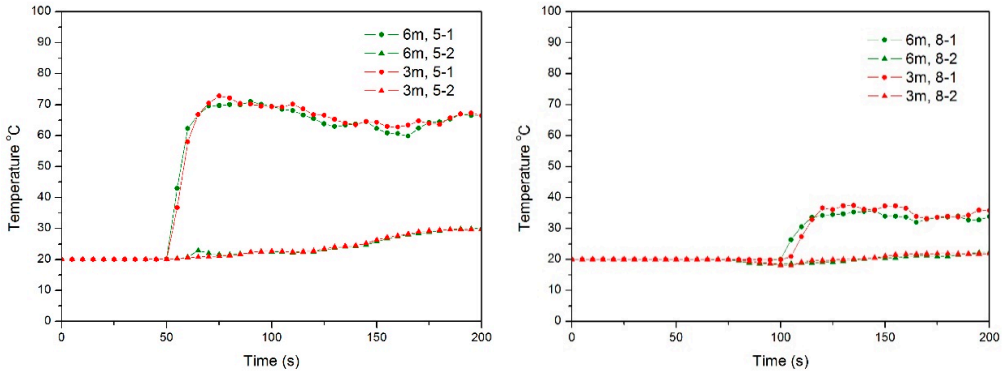

Figure 13. Temperature evolution at positions 5 (close to the fire source) and 8 (downstream of the water sprays) for test F-4.

4.4. Effect of Total Water Flow Rate

Sections 4.2 and 4.3 show that, under the conditions tested, nozzle arrangement and row spacing have limited effects on downstream temperature when the total water flow rate is insufficient. In these cases, the principal effect of the water mist is to cool the fire-induced smoke rather than to completely block it. Previous studies indicate that the total water flow rate is crucial to the smoke blocking performance. Therefore, this section examines the effect of total water flow rate by increasing the number of activated nozzles.

The HRR ranged from 1000 to 5000 kW, and the number of nozzles was increased from 12 to 54. Based on Sections 4.2 and 4.3, the number of nozzles per row and the row spacing were fixed at six nozzles per row and 6 m, respectively.

Figure 14 shows the temperature fields in the vertical mid-plane at x = 3.5 m for tests F-4, F-34, and F-44. For a 1000 kW fire, the number of nozzles was increased from 12 to 24 by activating additional nozzle rows. The results clearly show that increasing the number of activated nozzles, and therefore the total water flow rate, reduces the temperature downstream of the water mist curtain.

Figure 15 presents the longitudinal velocity component, vertical velocity component, and velocity vectors in the vertical plane at x = 3.5 m for tests F-4, F-34, and F-44. The reverse flow becomes more pronounced as more nozzle rows are activated. Figure 16 shows the longitudinal velocity profiles in the vertical plane at y = 80 m and y = 120 m. The

longitudinal velocity decreases as more nozzle rows are activated. Upstream of the water mist curtain, the velocity is approximately 1.5 m/s, whereas downstream of the curtain it decreases to approximately −0.3 m/s, indicating that air and smoke are entrained back toward the spray region. It is also worth noting that, although no reverse flow of fresh air occurs at the tunnel ceiling in tests F-4 and F-34, smoke is still found to flow back toward the water mist curtain in the middle and lower regions of the tunnel, $z < 3$ m. This behavior is beneficial for fire-smoke control.

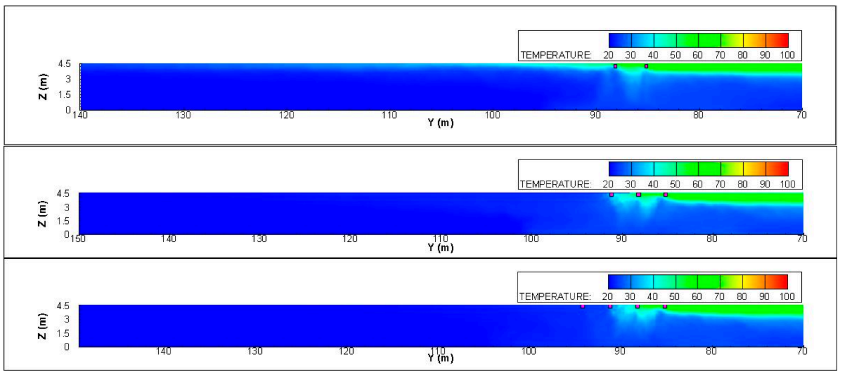

Figure 14. Temperature field in the vertical plane (x = 3.5 m) for tests F-4, F-34, and F-44 (from **top** to **bottom**). Values have been averaged over the steady-state period.

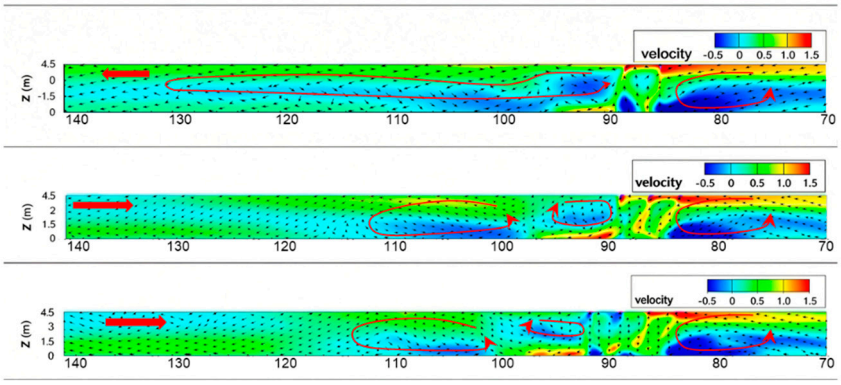

Figure 15. Longitudinal velocity component and velocity vectors in the vertical plane (x = 3.5 m) for tests F-4, F-34, and F-44. Values have been averaged over the steady-state period.

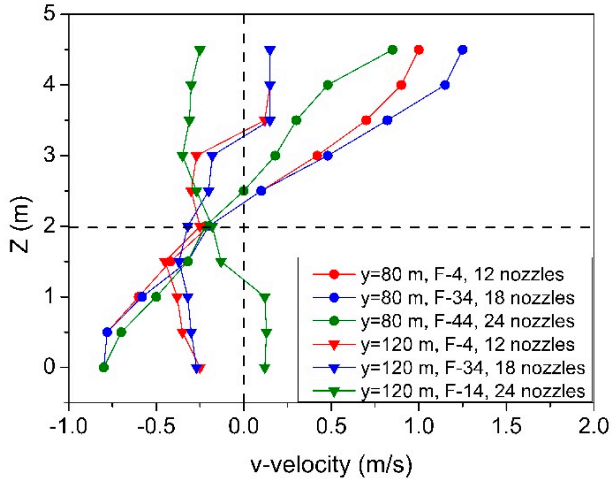

Figure 16. Velocity profiles in vertical plane (y = 80 and 120 m) for tests F-4, F-34, and F-44. Values have been averaged over the steady-state period.

Figure 17 quantifies the downstream temperatures at positions 10 and 11. As the number of activated nozzles increases, the downstream temperature decreases. When the number of nozzles is increased to 24, the downstream temperature approaches 20 °C, indicating effective smoke blocking under the tested 1000 kW condition.

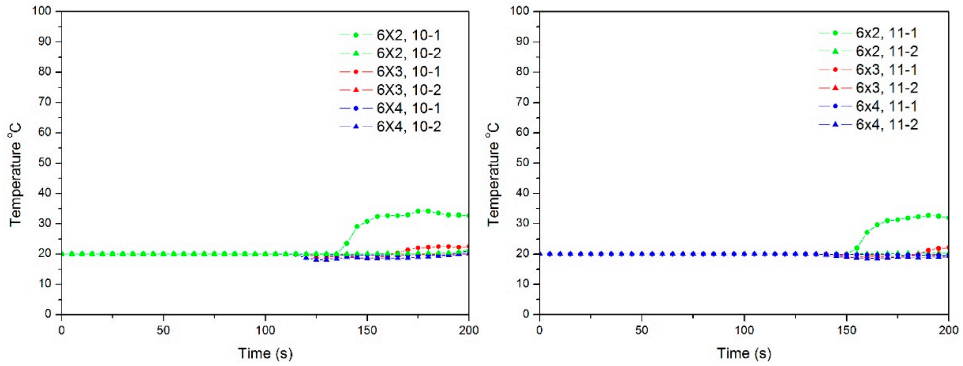

Figure 17. Temperature profiles for tests F-4, F-34, and F-44.

Therefore, it can be concluded that increasing the total water flow rate significantly enhances the smoke blocking effectiveness of the water mist curtain by enhancing the cooling effect and forming a reverse-flow, which makes it more difficult for fire-induced smoke to pass through the water mist zone.

4.5. Momentum-Ratio Criterion and Critical Condition

This section examines the relationship between the fire HRR and the water flow rate required for effective smoke blocking. As discussed above, when the water-mist momentum exceeds the horizontal momentum of the ceiling jet, the water mist curtain is more likely to prevent smoke from passing through the water mist curtain.

The ceiling-jet momentum can be calculated using Equation (2). The smoke-layer thickness near the water mist curtain was derived from the vertical temperature profiles. It is defined as the vertical distance from the tunnel ceiling to the point where the temperature decreases to one-half of the maximum temperature, as the dash line illustrates in Figure 18. According to the time-averaged temperature profile at the centreline of position 5 without water mist activation, the smoke-layer thickness is approximately 1.3 ± 0.2 m. The value of h_s = 1.3 m is used in the present study. The smoke-layer thickness increases with HRR: it is approximately 1.2 m for a 1000 kW fire and about 3.0 m for a 3000 kW fire.

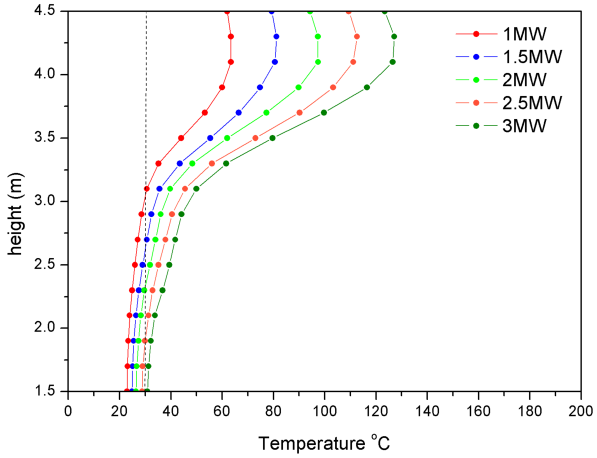

Figure 18. Profile of mean temperature in the vertical mid-plane at position 5. Values have been averaged over the steady-state period (150 s–200 s).

The water-mist momentum was estimated using Equation (1). The flow rate per nozzle was 7.1 L/min, and the nozzle orifice diameter was assumed to be 2.5 mm in the momentum calculation.

To explore this relationship, approximately 50 cases were simulated in this section. Figure 19 shows part of the simulation results that correspond to a sufficient smoke blocking effect. Averaged temperature profiles downstream of the water mist curtain at z = 4.4 m and z = 2.2 m are shown. In most cases, the downstream temperatures are 22 °C, indicating that the corresponding nozzle arrangements are sufficient for smoke blocking in these cases.

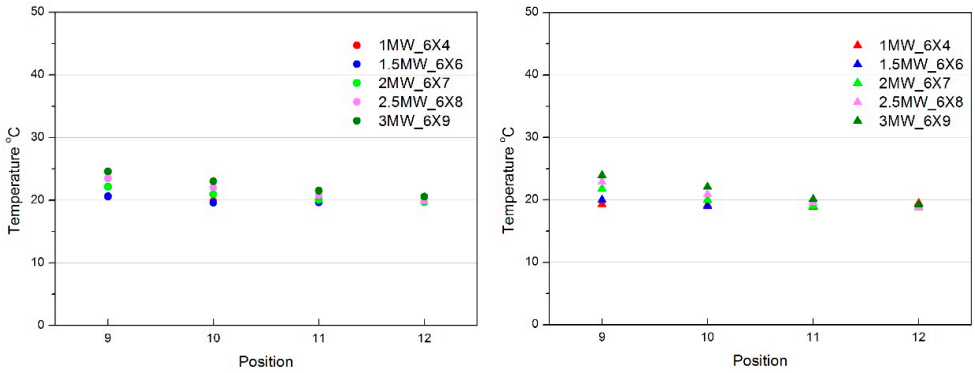

Figure 19. Averaged temperature in the mid-vertical plane at height z = 4.4 m (**left**) and z = 2.2 m (**right**) downstream of the water mist system.

Figure 20 shows the water mist curtain momentum required to effectively block fire smoke propagation and the corresponding fire smoke momentum at different fire heat release rates from extensive numerical simulations.

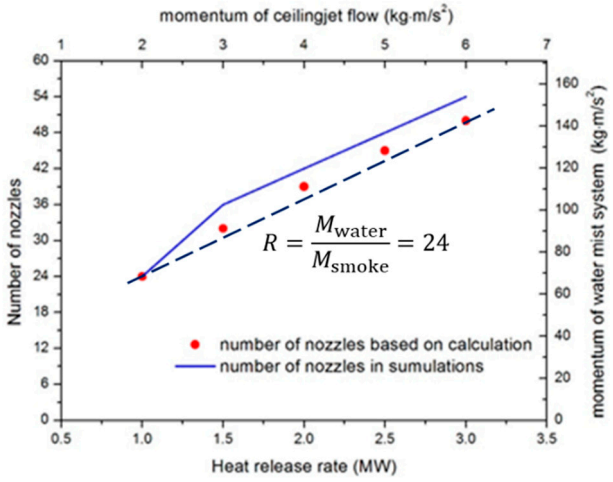

Figure 20. Correlation between the value of heat release rate (momentum of ceiling jet flow) and water flow rate (momentum of water mist system).

The black dashed line represents the constant momentum ratio $R = M_{water}/M_{smoke} = 24$; the blue line is the water mist momentum calculated from the nozzle quantities used in simulations, and the red dots are the theoretically required spray system momentum. As shown in the figure, both the required number of nozzles and the water mist momentum increase monotonically with the HRR, rising from approximately 24 nozzles at 1000 kW to about 48 nozzles at 3000 kW. This trend is consistent with the theoretical analysis; a stronger water mist curtain is required as the fire size increases. However, the theoretical analysis slightly underestimates the value, which is likely caused by the six-nozzle increment between

simulated cases. In general, the proposed momentum-ratio criterion offers a reasonable preliminary basis to estimate the required water mist curtain capacity under different fire scenarios.

It must be emphasized that this momentum value is a bulk estimation of the droplet momentum of the water mist curtain system, and the ceiling-jet momentum uses the empirical correlation of Kurioka et al. [2] with an assumed smoke-layer thickness inferred from temperature profiles. Moreover, the estimation of the smoke layer thickness also introduces an uncertainty (error) of approximately 10%. As mentioned in Sections 4.2 and 4.3, the arrangement of the nozzle (including the number of nozzles per row, the number of nozzle rows, and distance between each nozzle) affects the smoke-blocking effectiveness. Therefore, even if the total momentum of the water mist curtain system can be estimated, the specific nozzle parameters of the water mist curtain system still need to be discussed carefully.

5. Conclusions

This study investigated the smoke blocking performance of a water mist curtain in tunnels using small-scale experiments and full-scale FDS simulations. The main conclusions are as follows:

(1) Small-scale tests confirm that a water mist curtain can reduce the downstream spread of fire-induced heat and smoke under natural ventilation, and the full-scale simulations reproduce the key flow features observed in the reduced-scale tests, with relative temperature deviations of less than 8% at mid-height and 30% at positions near the water mist region subjected to complex flow field and heat transfer processes.

(2) When the total water flow rate is insufficient, changing the nozzle arrangement—including the number of nozzles per row and row spacing—exerts only a limited effect on the downstream temperature by no more than 23% (maximum temperature difference of approximately 7 °C). As smoke penetrates the water mist curtain, increasing the water mist coverage does not guarantee a lower temperature downstream of the water mist curtain.

(3) The water flow rate is the key parameter that determines the effectiveness of a water mist curtain in blocking fire-induced smoke. Increasing the total water flow rate significantly improves the smoke blocking effect by enhancing the cooling effect and inducing a reverse-flow region near the water mist curtain. For the cases studied, the temperature downstream of the water mist curtain dropped from 35 °C to 22 °C, which was considered to indicate that the fire-induced smoke was sufficiently blocked.

(4) Based on the theoretical analysis and simulation results, a momentum-based criterion, a dimensionless momentum ratio, $R = \frac{M_w}{M_s}$, is proposed to evaluate the smoke containment capability, and a critical value of $R = 24$ is identified for the tested conditions (tunnel geometry of 11 m × 4 m, the tested nozzle configuration, natural ventilation, and HRRs of 1000–5000 kW). These findings provide a preliminary basis for the design and optimization of water mist curtains in road tunnels.

It should be noted that this study adopts the widely used Froude criterion for model scaling, which means that the requirement for the Reynolds number is relaxed. This simplification may cause deviations in simulation results in this paper. Moreover, the momentum criterion proposed in this paper is based on limited fire scenarios. Therefore, this criterion can only be used as a preliminary design indicator. More validation work, including full-scale experiments, is required.

Author Contributions: Conceptualization, J.S.; methodology, J.S.; software, J.S.; validation, J.W.; formal analysis, Z.G.; investigation, J.S.; resources, J.S.; data curation, J.S.; writing—original draft preparation, J.S.; writing—review and editing, J.W.; visualization, Z.G.; supervision, J.W.; project

administration, J.S.; funding acquisition, J.S. and J.W. All authors have read and agreed to the published version of the manuscript.

Funding: This work is supported by the "Natural Science Foundation of Hubei Province", No. 2024AFB174; "Scientific Research Program of Hubei Provincial Department of Education", Nos. Q20251616 and B2023060; and "Open Projects Foundation of State Key Laboratory of Bridge Intelligent and Green Construction", No. BIGCSKL25-06-YF.

Data Availability Statement: The data presented in this study are available on request from the corresponding author.

Conflicts of Interest: The authors declare no conflict of interest.

References

1. Beard, A.N.; Carvel, R.O. *Handbook of Tunnel Fire Safety*, 2nd ed.; ICE Publishing: London, UK, 2012.
2. Kurioka, H.; Oka, Y.; Satoh, H.; Sugawa, O. Fire properties in near field of square fire source with longitudinal ventilation in tunnels. *Fire Saf. J.* **2003**, *38*, 319–340. [CrossRef]
3. Hu, L.H.; Chen, L.; Wu, L.; Li, Y.; Zhang, J.; Meng, N. An experimental investigation and correlation on buoyant gas temperature below ceiling in a slopping tunnel fire. *Appl. Therm. Eng.* **2013**, *51*, 246–254. [CrossRef]
4. Oka, Y.; Imazeki, O. Temperature distribution within a ceiling jet propagating in an inclined flat-ceilinged tunnel with natural ventilation. *Fire Saf. J.* **2015**, *71*, 20–33. [CrossRef]
5. Hu, L.H.; Huo, R.; Peng, W.; Chow, W.; Yang, R. On the maximum smoke temperature under the ceiling in tunnel fires. *Tunn. Undergr. Space Technol.* **2006**, *21*, 650–655. [CrossRef]
6. Hu, L.H.; Huo, R.; Li, Y.Z.; Wang, H.B.; Chow, W.K. Full-scale burning tests on studying smoke temperature and velocity along a corridor. *Tunn. Undergr. Space Technol.* **2005**, *20*, 223–229. [CrossRef]
7. Amano, R.; Izushi, Y.; Kurioka, H.; Sato, H.; Kuwana, H.; Tsuruda, T.; Ogawa, Y.; Suzuki, T. Water screen fire disaster prevention system in underground space. In Proceedings of the 6th Asia-Oceania Symposium on Fire Science and Technology, Daegu, Republic of Korea, 17–20 May 2004.
8. Sun, J.; Fang, Z.; Tang, Z.; Beji, T.; Merci, B. Experimental study of the effectiveness of a water system in blocking fire-induced smoke and heat in reduced-scale tunnel tests. *Tunn. Undergr. Space Technol.* **2016**, *56*, 34–44. [CrossRef]
9. Sun, J.; Tang, Z.; Fang, Z.; Beji, T.; Merci, B. Flow fields induced by longitudinal ventilation and water spray system in reduced-scale tunnel fires. *Tunn. Undergr. Space Technol.* **2020**, *104*, 103543. [CrossRef]
10. Sun, J.; Fang, Z.; Beji, T.; Merci, B. Interpretation of flow fields induced by water spray systems in reduced-scale tunnel fire experiments by means of CFD simulations. *Tunn. Undergr. Space Technol.* **2018**, *81*, 94–102. [CrossRef]
11. Liang, Q.; Li, Y.; Li, J.; Xu, H.; Li, K. Numerical studies on the smoke control by water mist screens with transverse ventilation in tunnel fires. *Tunn. Undergr. Space Technol.* **2017**, *64*, 177–183. [CrossRef]
12. Liu, Y.; Li, Q.; Tang, Z.; Fang, Z. Effect of water mist system settings on fire and upstream smoke control in a longitudinally ventilated tunnel. *Tunn. Undergr. Space Technol.* **2025**, *155*, 106234. [CrossRef]
13. Gao, Z.; Wang, P.; Wang, P.; Peng, L. The impact of water mist nozzle arrangements on the back-layering length in tunnel fires. *J. Therm. Anal. Calorim.* **2026**. [CrossRef]
14. Kan, D.; Wang, P.; Wang, P.; Peng, L. Full-scale experimental study on the smoke and thermal insulation of a water mist fire extinguishing system in a short road tunnel with natural ventilation. *Tunn. Undergr. Space Technol.* **2025**, *158*, 106414. [CrossRef]
15. Chen, Y.; Jia, J.; Che, G.; Zhu, Z.; Shen, Z. Simulation research on the temperature distribution and smoke control in tunnel fires under a water curtain system. *Geomat. Nat. Hazards Risk* **2023**, *14*, 2225687. [CrossRef]
16. Li, Q.; Tang, Z.; Fang, Z.; Yuan, J.; Wang, J. Experimental study of the effectiveness of a water mist segment system in blocking fire-induced smoke and heat in mid-scale tunnel tests. *Tunn. Undergr. Space Technol.* **2019**, *88*, 237–249. [CrossRef]
17. Wang, J.; Wei, Y.; Xie, Z.; Jiang, X.; Zhang, H.; Lu, K. Influence of the water spray flow rate and angle on the critical velocity in tunnels with longitudinal ventilation. *Energy* **2020**, *190*, 116466. [CrossRef]
18. Grant, G.; Brenton, J.; Drysdale, D. Fire suppression by water sprays. *Prog. Energy Combust. Sci.* **2000**, *26*, 79–130. [CrossRef]
19. Alenezi, M.H.; Sadek, H. Fire-suppression performance of high-pressure water mist system inside scaled-down road tunnel section. *J. Eng. Res.* **2023**, *11*, 100024. [CrossRef]
20. Ingason, H. Model scale tunnel tests with water spray. *Fire Saf. J.* **2008**, *43*, 512–528. [CrossRef]
21. Lee, J. Numerical analysis of how ventilation conditions impact compartment fire suppression by water mist. *Ann. Nucl. Energy* **2020**, *136*, 107021. [CrossRef]
22. Fan, C.; Bu, R.; Xie, X.; Zhou, Y. Full-scale experimental study on water mist fire suppression in a railway tunnel rescue station: Temperature distribution characteristics. *Process Saf. Environ. Prot.* **2021**, *146*, 396–411. [CrossRef]

23. Blanchard, E.; Morlon, R.; Parent, G.; Fromy, P.; Boulet, P.; Borgiallo, D. Experimental Study of the Interaction Between Water Sprays and Smoke Layer. *Fire Technol.* **2018**, *54*, 479–501. [CrossRef]
24. Beji, T.; Ebrahimzadeh, S.; Maragkos, G.; Merci, B. Numerical modelling of the interaction between water sprays and hot air jets-Part II: Two-phase flow simulations. *Fire Saf. J.* **2018**, *96*, 143–152. [CrossRef]
25. Hardy, L.; Collin, A.; Suzanne, M.; Collin, A.; Suzanne, M.; Erez, G.; Mehaddi, R.; Boulet, P. Study of the Interactions Between a Water Spray and a Moving Layer of Hot Smoke. *Fire Technol.* **2025**, *61*, 513–540. [CrossRef]
26. Mehaddi, R.; Collin, A.; Boulet, P.; Acem, Z.; Telassamou, J.; Becker, S.; Demeurie, F.; Morel, J.-Y. Use of a water mist for smoke confinement and radiation shielding in case of fire during tunnel construction. *Int. J. Therm. Sci.* **2020**, *148*, 106156. [CrossRef]
27. Li, Y.Z.; Ingason, H. Model scale tunnel fire tests with automatic sprinkler. *Fire Saf. J.* **2013**, *61*, 298–313. [CrossRef]
28. McGrattan, K.; Hostikka, S.; McDermott, R.; Floyd, J.; Weinschenk, C.; Overholt, K. Fire Dynamics Simulator User's Guide. In *NIST Special Publication 1019*, 6th ed.; National Institute of Standards and Technology: Gaithersburg, MD, USA, 2013.
29. McGrattan, K.B.; Baum, H.R.; Rehm, R.G. Large eddy simulations of smoke movement. *Fire Saf. J.* **1998**, *30*, 161–178. [CrossRef]
30. Van Maele, K.; Merci, B. Application of RANS and LES field simulations to predict the critical ventilation velocity in longitudinally ventilated horizontal tunnels. *Fire Saf. J.* **2008**, *43*, 598–609. [CrossRef]

Disclaimer/Publisher's Note: The statements, opinions and data contained in all publications are solely those of the individual author(s) and contributor(s) and not of MDPI and/or the editor(s). MDPI and/or the editor(s) disclaim responsibility for any injury to people or property resulting from any ideas, methods, instructions or products referred to in the content.